AGU PUBLICATIONS

JGR

Journal of Geophysical Research: Oceans

RESEARCH ARTICLE

10.1002/2015JC011533

Special Section:
Physical Processes Responsible for Material Transport in the Gulf of Mexico for Oil Spill Applications

Surface dynamics of crude and weathered oil in the presence of dispersants: Laboratory experiment and numerical simulation

Alexander V. Soloviev[1,2], Brian. K. Haus[2], Michael G. McGauley[1], Cayla W. Dean[1], David G. Ortiz-Suslow[2], Nathan J. M. Laxague[2], and Tamay M. Özgökmen[2]

[1]Halmos College of Natural Science and Oceanography, Nova Southeastern University, Dania Beach, Florida, USA, [2]Rosenstiel School of Marine and Atmospheric Science, University of Miami, Miami, Florida, USA

Key Points:
- Small-scale dynamics of surface oil spills are a critical component of hydrocarbon transport models
- Laboratory and computational experiments were conducted with crude and high viscosity oil and dispersant
- A new interpretation of the effect of dispersants including capillary forces has been developed

Citation:
Soloviev, A. V., B. K. Haus, M. G. McGauley, C. W. Dean, D. G. Ortiz-Suslow, N. J. M. Laxague, and T. M. Özgökmen (2016), Surface dynamics of crude and weathered oil in the presence of dispersants: Laboratory experiment and numerical simulation, *J. Geophys. Res. Oceans*, *121*, 3502–3516, doi:10.1002/2015JC011533.

Received 7 DEC 2015
Accepted 25 APR 2016
Accepted article online 30 APR 2016
Published online 27 MAY 2016

Abstract Marine oil spills can have dire consequences for the environment. Research on their dynamics is important for the well-being of coastal communities and their economies. Propagation of oil spills is a very complex physical-chemical process. As seen during the Deepwater Horizon event in the Gulf of Mexico during 2010, one of the critical problems remaining for prediction of oil transport and dispersion in the marine environment is the small-scale structure and dynamics of surface oil spills. The laboratory experiments conducted in this work were focused on understanding the differences between the dynamics of crude and weathered oil spills and the effect of dispersants. After deposition on the still water surface, a drop of crude oil quickly spread into a thin slick; while at the same time, a drop of machine (proxy for weathered) oil did not show significant evolution. Subsequent application of dispersant to the crude oil slick resulted in a quick contraction or fragmentation of the slick into narrow wedges and tiny drops. Notably, the slick of machine oil did not show significant change in size or topology after spraying dispersant. An advanced multi-phase, volume of fluid computational fluid dynamics model, incorporating capillary forces, was able to explain some of the features observed in the laboratory experiment. As a result of the laboratory and modeling experiments, the new interpretation of the effect of dispersant on the oil dispersion process including capillary effects has been proposed, which is expected to lead to improved oil spill models and response strategies.

1. Introduction

Recent oil spill disasters have demonstrated the importance of research on oil propagation and dispersion in the oceanic environment [*Joye and MacDonald*, 2010]. Oil, when spilled on water, spreads outward on the water surface in the form of a thin slick, which has been known for a long time [see e.g., *Franklin*, 1774]. Spreading and drifting of the oil spill on the sea surface occurs due to gravity, viscosity, and interfacial tension forces as well as wind-wave actions and currents. A variety of regimes of oil transport take place, depending on wind/wave conditions, spill age, oil characteristics, and the use of dispersants. The oil, especially crude oil, can also react with salt water producing surfactants at the oil-water interface, which affect the interfacial tension coefficient [*van Nierop et al*., 2006].

One of the first oil spreading models was introduced by *Fay* [1969], followed by *Hoult* [1972] and *Fannelop and Waldman* [1972]. These authors considered the spread of an oil slick from a theoretical viewpoint to calculate the extent of the spread of oil slicks onto calm water as a function of time.

The initial breakup of the oil drop is determined by the drop placement process [*Eggers*, 1997]. After the initial moment of the oil drop contact with the water surface, a triple junction surface of oil, water, and air phases occurs assuming that the liquid phases are immiscible [see e.g., *Miksis and Vanden-Broeck*, 2001]. The triple junction is a point in two dimensions and a line in three dimensions. The surface tension forces at the triple junction influence the process of oil drop spreading on the water surface.

Figure 1 shows a two-dimensional projection of three interfaces between air, water, and oil forming a triple junction point. Near the triple junction, the initial distribution of the fluids takes the shape of three wedges

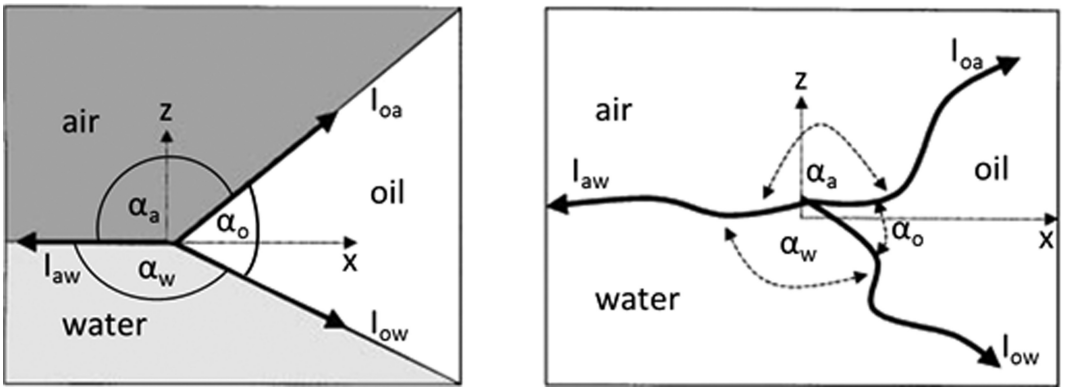

Figure 1. A two-dimensional projection of three inviscid fluids in the form of three wedges forming a triple junction: (a) The initial configuration at t = 0 and (b) a dynamic triple junction for t > 0. (Adapted for air-oil-interface system from *Miksis and Vanden-Broeck* [2001].) The air-water, oil-air, and oil-water interfaces are denoted as l_{aw}, l_{oa}, and l_{ow}, respectively.

(Figure 1a). After the triple junction formation, the local interface shapes start adjustment in order to balance all local forces (Figure 1b).

Dispersant deposition or surfactant presence (or removal) can cause the surface tension between some fluid pairs to rapidly change, prompting deformation of the interfaces. The resulting imbalance of forces at the triple junction will initiate the motion of the interfaces and corresponding change of the oil droplet shape, until a new state is attained [*Miksis and Vanden-Broeck*, 2001]. (Oil viscosity is also an important parameter in the process of contraction and expansion, with the crude oil responding much faster than the weathered oil - see Discussion).

The contact angles between the fluids should obey the following trivial condition:

$$\alpha_a+\alpha_o+\alpha_w=2\pi,$$

where α_a, α_o, and α_w are the dihedral contact angles between air, oil, and water, as shown in Figure 1. Equilibrium between all three phases is achieved under the following conditions [*Rowlinson and Widom*, 1982]:

$$\sigma_{ao}+\sigma_{ow}\cos\alpha_o+\sigma_{aw}\cos\alpha_a=0,$$

$$\sigma_{ao}\cos\alpha_o+\sigma_{ow}+\sigma_{aw}\cos\alpha_w=0,$$

$$\sigma_{ao}\cos\alpha_a+\sigma_{ow}\cos\alpha_w+\sigma_{aw}=0,$$

where σ_{aw}, σ_{ao}, and σ_{ow} are the air-water, air-oil, and oil-water interfacial tensions, respectively.

Evolution of an oil drop on the water surface can be characterized by the spreading coefficient [*Harkins*, 1952]:

$$S\equiv\sigma_{aw}-\sigma_{oa}-\sigma_{ow}. \quad (1)$$

For $S\geq 0$, the oil droplet has no equilibrium state and can completely spread, or "wet," the air-water interface. *Dipietro et al*. [1978] and *Foda and Cox* [1980] developed a theory for the spreading of a droplet in the completely wetting case. They, however, had to include in the model the so-called leading precursor (a monolayer) film driven by surface tension gradients, which allowed them to obtain steady and similarity solutions. The problem is that as complete wetting is approached, the three-phase line begins to disappear and the question may arise whether the effect of interfacial tension and tension of the three-phase line on the drop spreading would vanish as well [*Amirfazli and Neumann*, 2004]. For $S<0$, an equilibrium configuration arises, which takes the form of a sessile lens [*Hoult*, 1972] and does not require the additional assumption of a monolayer precursor.

As already mentioned, the balance of interfacial tensions between three phases shown in Figure 1 is a projection of the triple junction on a plane. In three-dimensional space, the three phases produce a contact line, which results in an additional tension, the so-called line tension. *Gibbs* [1961] mentioned "a certain linear tension" in his theory of capillarity. *Langmuir* [1933] introduced the concept of the line tension at the

three-phase contact line considering a hydrocarbon sessile lens on the water surface. *Pujado and Scriven* [1972], however, found serious errors in Langmuir's analysis and downplayed the importance of the line tension. Subsequent work, nevertheless, has shown that the line tension can be a factor in sessile lens dynamics [*Amirfazli and Neumann*, 2004].

The line tension force γ depends on the curvature radius r of the three-phase contact line on the water surface, as

$$\gamma \sim 1/r. \tag{2}$$

According to (2), the effect of line tension increases with reduction of the oil drop size. The line tension can, therefore, be of critical importance for the process of oil fragmentation and dispersion that takes place on microscale. Theoretical and experimental estimations of the line tension still differ dramatically. Theoreticians declare that line tension can have either a positive or a negative sign. In experimental studies of liquid lens values (excluding the near wetting studies), positive line tensions as high as 10^{-6} N were reported [*Amirfazli and Neumann*, 2004].

For the case of relatively low viscosity fluids, like crude oil and water, the motion on sufficiently small scales is expected to be controlled primarily by surface tension forces. The spreading of oil is driven by capillary forces for small drops and by inertia and gravity for large ones. The crossover radius between these two regimes is the interfacial capillary length, which is defined as follows [*Bacri et al*., 1996]:

$$r_c = \sqrt{\sigma_{ef}/(\tilde{\rho} g)}, \tag{3}$$

where σ_{ef} is an effective interfacial tension determined from equation ${\sigma_{ef}}^{-1} = \sigma_{ow}^{-1} + {\sigma_{ao}}^{-1}$,

$\tilde{\rho}$ is the effective density determined from equation $\tilde{\rho} = \rho_o(1 - \rho_o/\rho_w)$, and ρ_o, ρ_w are the density of oil and water, respectively.

Surface tension forces are also at the origin of the Marangoni effect [see e.g., *Pismen*, 2002]. This phenomenon initiates mass transfer along an interface between two fluids if there is a surface tension gradient along this interface.

The Marangoni effect on the oil spill propagation and dispersion has not yet been thoroughly investigated. There are nevertheless indications that it is of primary importance for understanding the process of oil dispersion. An example is given in Figure 2. The application of dispersant to the water surface around the crude oil slick dramatically decreases the air-water surface tension. As a result, the spreading factor S becomes negative, forcing the surface slick to contract to a new equilibrium state (as sketched in Figure 2). Water circulation at the oil-water interface flushes away the surfactant diffusion sublayer produced by diffusion or chemical reactions and between crude oil and water. Reduction of the surfactant concentration results in an increase of the interfacial tension between oil and water further reducing the spreading coefficient S to a more negative value. In the process of adjustment of the dihedral contact angles to a new equilibrium state similar to that schematically shown in Figure 2, the oil slick rapidly contracts. For immiscible fluids, the balance of interfacial tensions at the triple junction can be interpreted as an extreme form of the Marangoni effect.

The literature review suggests that propagation of oil spills is a very complex physical-chemical process. Most small-scale processes, like capillarity effects and the triple junction in the air-water-oil system, have been analyzed in a two-dimensional perspective only, imposing limitations on the analysis and modeling of oil spills. In this work, we focus on the three-dimensional aspects of this problem associated with interfacial tension, oil viscosity (age), and application of dispersants. Better knowledge of these small-scale processes is expected to help improve subgrid-scale parameterizations for large-scale oil transport models.

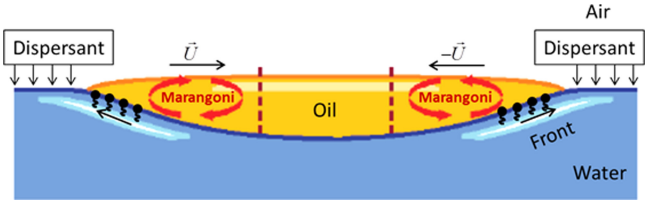

Figure 2. Schematic representation of crude oil patch contraction after the application of dispersants to the water surface around the slick. The diagram is compiled based on *Bush* [2013].

Our approach combines laboratory experiments with an advanced

computational fluid dynamics model incorporating small-scale physics and capillary effects. Laboratory experiments serve as a verification of the model results. This approach can help to extrapolate the laboratory results to the ocean environment including wind/wave mixing, near surface currents, chemical reactions of oil with saltwater and dispersants, weathering, evaporation, dissolution, and emulsification of oil spills.

The structure of the paper is as follows: section 2 describes the laboratory experiments, section 3 presents the computational fluid dynamics volume of fluid multiphase model, and section 4 describes the results of numerical simulations conducted in parallel with the laboratory experiments. Section 5 is the discussion of laboratory and numerical experiments, and section 6 contains the main conclusions of this work.

2. Laboratory Experiments

In this work, two laboratory experiments on oil spill dynamics were conducted at the University of Miami Rosenstiel School of Marine Science air-sea interaction facility SUrge STructure Atmosphere INteraction (SUSTAIN) (http://sustain.rsmas.miami.edu/). The experiments with oil and dispersants were done in a small acrylic tank (Figure 3). The experiments were conducted with crude and machine oil. Oil weathering is the sum of the physical and biological processes acting on oil, which change the chemical composition and physical properties, such as viscosity, over time. The crude oil in the laboratory experiment was represented by the Macondo surrogate oil. We have used machine oil "Valvoline 20W-50 Premium Conventional Motor Oil" as a proxy for weathered oil based on the high molecular viscosity of machine oils, typical for weathered oil. The viscosity of the machine oil used in these experiments is estimated as 0.4 kg $m^{-1}s^{-1}$ (400 cSt) at 25°C [*Stachowiak et al*., 2011].

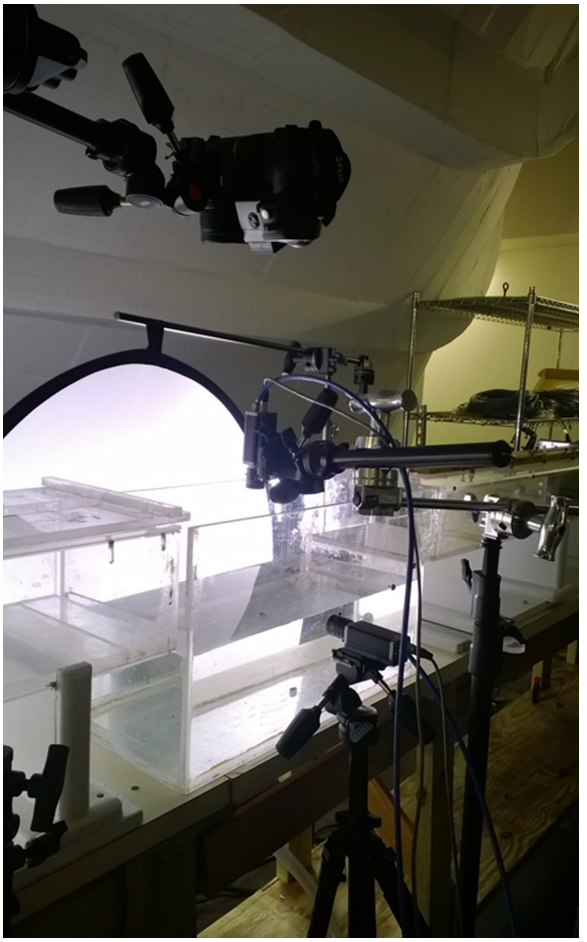

Figure 3. A small acrylic tank, 0.57 m long × 0.27 m wide × 0.35 m high, for oil slick and dispersant experiments at SUSTAIN.

The first experiment was conducted on 13 May 2014 and included only a top-view camera. The laboratory experiments conducted on 15 October 2015 included a side-view camera, top-view camera, and infrared camera. For the experiment on 15 October 2015, the side and top-view cameras were calibrated in order to measure oil slick dimensions. An infrared camera is an effective tool to observe surface tension effects, because the image captures only a few-micrometer thick surface layer of water, thus emphasizing surface tension effects.

Crude and machine oil drops were created using syringes. In several experiments the drops were near simultaneously released from a few centimeter height above the water surface with horizontal spacing of roughly 10 cm. For the experiments involving dispersants, we used the FFT-Solution™ dispersant supplied by *Fog Free Technologies*. After each trial the surface oil was removed using oil-absorbing sheets, then the basin was completely drained and cleaned before re-filling with new water.

2.1. Experiments on 13 May 2014

Laboratory experiments conducted on 13 May 2014 are listed in Table 1. The images

Table 1. Laboratory Experiment Conducted on 13 May 2014 in Fresh Water

Oil and Dispersant Type	Related Figures
Crude[a] and machine[b] oil	4
Crude[a] and machine[b] oil, dispersant[c]	5

[a]Macondo surrogate oil.
[b]Valvoline 20W-50 Premium Conventional Motor Oil.
[c]FFT-Solution™.

shown in Figures 4 and 5 are frame captures from 4.13 megapixel, 24 Hz imagery collected via GoPro camera. The camera was mounted above the tank and set to use the 90° field of view in order to reduce the wide-angle distortion typical of these cameras. Figure 4 shows drops of machine versus crude oil approximately 25 s after oil drop releases. The crude oil slick rapidly expanded and in several seconds formed a very thin film on the water surface of a somewhat irregular shape with a characteristic length scale of about 5 cm. This expansion can be due to disappearance of the triple line and line tension under complete wetting conditions ($S \geq 0$) [*Amirfazli and Neumann*, 2004]. Alternatively, the spreading can be powered by the Marangoni force, forming a precursor film (the effect previously referred to by *Dipietro et al.* [1978] and *Foda and Cox* [1980]).

In contrast, the machine oil slick did not change significantly during the same time period as the crude oil expanded. This slick was of a circular shape with diameter 0.8 cm (Figure 4).

The reason is that machine oil has much higher molecular viscosity and cannot respond rapidly to the disappearance of the triple line and line tensions. The Marangoni effect is suppressed by the high viscosity of the machine oil. Note that the characteristic velocity of Marangoni flows can be scaled as $u=\Delta\sigma/\mu$, where $\Delta\sigma$ is the change of surface tension between phases and μ is the dynamic viscosity of the fluid [see e.g., *Tam et al.*, 2009]. The ratio of characteristic velocity scales for machine (u_m) and crude (u_c) oil droplet spreading is then inversely proportional to the ratio of their viscosities:

$$u_m/u_c \sim \mu_c/\mu_m = O(10^{-1}). \quad (4)$$

Since the viscosity of machine oil is much higher than that of crude oil, the characteristic velocity scale for the machine oil spreading is much smaller than for the crude oil.

The effect of dispersants was tested by adding the FFT-Solution™ dispersant on the water surface outside of oil slicks. In the experiment shown in Figure 5, multiple drops of crude and machine oil were initially released (Figure 5a). The characteristic length scale of the crude oil slick was on the order of 10 cm, and machine oil slicks were on the order of 1 cm. Figure 5 shows a succession of images of the crude and machine the oil slicks after the application of dispersant. The dispersant was applied on one side of the crude oil slick and on one side of the machine oil slick. The crude oil slick then began contracting (Figure 5b) and evolved into a wedge of approximately 1 cm wide and 10 cm long (Figure 5c). The machine oil plumes did not change significantly after application of the dispersant.

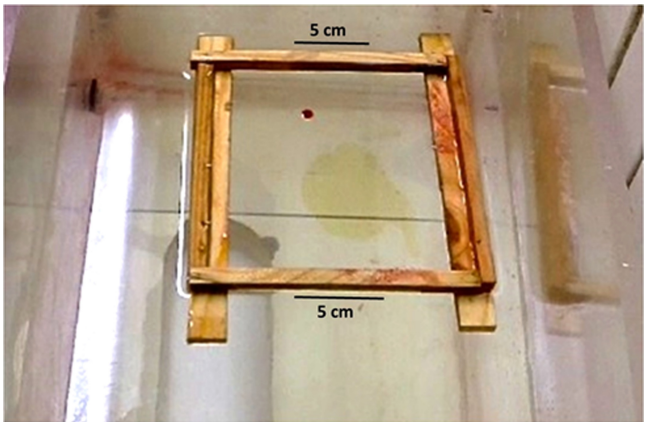

Figure 4. Machine (red) versus crude (brown film) oil slick on clean water surface without wind forcing in tank of width 27 cm. Image was taken shortly after simultaneous release of oil drops. The wooden frame was placed on the water surface in order to have a length scale. The linear scale is shown at two locations because the camera was at an angle to the water surface.

Our interpretation of the observed difference between crude and machine oil dynamics is as follows: Application of dispersant significantly changed the air-water surface tension; as a result, the spreading coefficient S became negative and favored oil slick contraction. The surface tension and Marangoni forces then pulled the surface oil slick into narrow wedges or compact drops. At the same time, the machine oil slick apparently was not strongly affected by the application of dispersants (Figures 5a-5c), which can be explained by relatively large molecular viscosity suppressing interfacial and Marangoni forces (see equation (5)).

One interesting conclusion following from these simple and largely

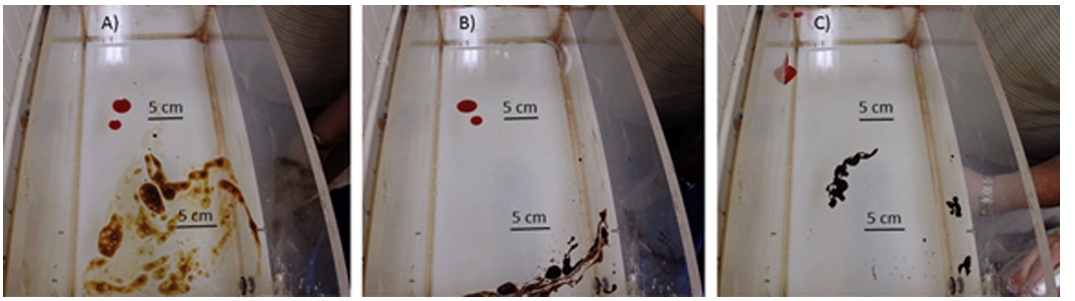

Figure 5. (a) Machine (red) and crude (dark brown) oil just released; (b) Immediately after 10% solution of FFT-Solution™ oil dispersant applied aerially from a spray bottle to the water surface; (c) Crude oil contracted, while the machine oil did not change much in diameter, though moved and "glued" to the tank wall. The linear scales are shown at two locations because the camera was at an angle to the water surface. The image was also somewhat distorted due to the fish-eye lens.

qualitative experiments is that application of dispersants outside of the crude oil slick results in its contraction rather than fragmentation. This is, however, different in the case when dispersant is applied onto the oil slick (see next section).

2.2. Experiments on 15 October 2015

In this set of experiments, which is summarized in Table 2, we released both crude and machine oil drops nearly simultaneously, as in the experiment on 13 May 2014, or separately, in order to avoid their interactions. Another difference from the experiment conducted on 13 May 2014 was that dispersant was applied (sprayed) directly on the oil slick rather than outside the slick. The water used was room temperature, 10 μm filtered seawater.

Figure 6 shows the crude oil slick rapidly spreading on the seawater surface. At the same time the machine oil barely spread during the 2 s time period (Figure 7). These observations are qualitatively consistent with the lab experiment on 13 May 2014 (Figure 4).

The effect of dispersants was tested by adding the 10% FFT-Solution™ dispersant on the water surface by spraying it directly on the oil slicks. Figure 8 shows visual and infrared images of the crude and machine oil slicks before and after the application of dispersant. For this test, we dropped the crude and machine oil, approximately 18 s before images shown in Figures 8a and 8c.

The crude oil slick almost instantaneously fragmented into narrow wedges and small drops, within a few tenths of a second (Figures 8b and 8d). This process was spectacular in the infrared imagery demonstrating the dramatic effect of surface tension on the microscale. Note that the IR imagery is formed in a micrometer-scale surface layer, where tension forces are most effective.

In this experiment, the diameter of the crude oil drop before application of dispersant was 10.9 cm. The size of the filaments of crude oil after application of dispersant ranged from sub-millimeter to centimeter scales. (Note that the resolution of the visual camera was 0.027 cm/pixel.) The diameter of the machine oil drop before application of dispersant was 1.2 cm and 0.8 cm after application of dispersant.

Table 2. Laboratory Experiment Conducted on 15 October 2015[a]

Case	Approximate Time	Oil and Dispersant Type	Related Figures
1	14:15	Crude[b]	6, 14
2	14:30	Crude[b]	14
3	14:45	Machine[c]	7, 14
4	15:15	Crude[b] and machine[c], dispersant[d]	8
5	15:30	Calibration test	

[a]Note that cases 1, 2, and 3 included single oil drop releases, either crude or machine; while, case 4 included both oil type drops released near simultaneously. Case 5 included placing a wooden object of known size on the water surface in the view of the camera in order to validate the camera calibration. Water temperature was 25°C; salinity, 32.5 psu.
[b]Macondo surrogate oil.
[c]Valvoline 20W-50 Premium Conventional Motor Oil.
[d]FFT-Solution™.

Our interpretation of the fragmentation of the crude oil slick is that after spraying, dispersant drops penetrated into the crude oil slick producing strong gradients of surface tension. The resulting Marangoni force caused the almost instantaneous fragmentation of the crude oil slick. The machine oil drop in response to dispersant application somewhat reduced in size but without

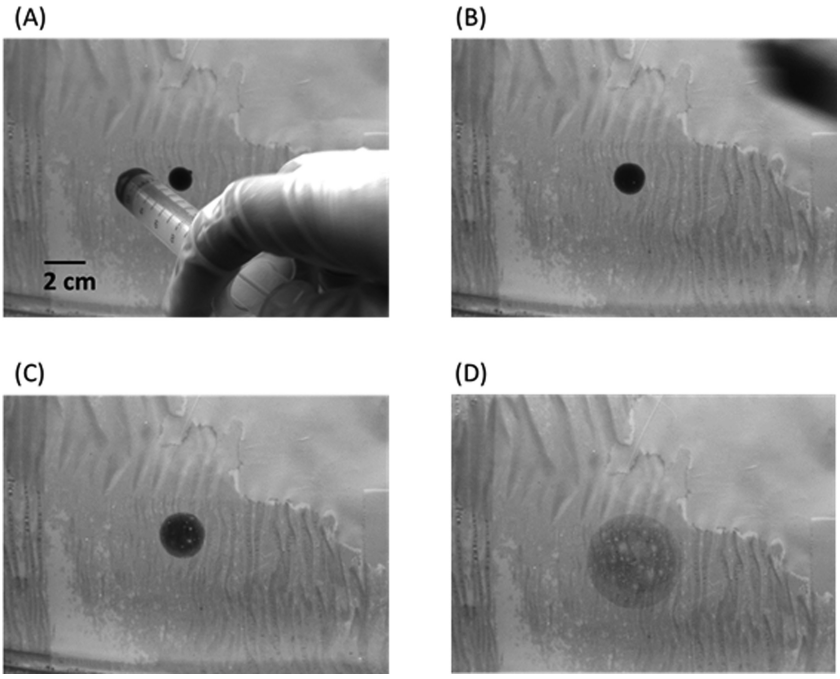

Figure 6. Crude oil slick (A) 0.33 s, (B) 0.60 s, (C) 1.00 s, and (D) 2.00 s after release on the water surface.

any fragmentation. The machine oil drop was pushed toward a side of the tank and eventually "glued" to the tank wall, presumably due to the Marangoni effect, similar to the case shown in Figure 5c.

Dispersant cannot quickly penetrate into the machine oil plume due to low molecular diffusivity of the machine oil. Since the machine oil drop did not spread much before dispersant application (Figure 5), a portion of the dispersant ended up on the edges of the plume. Marangoni effect at the machine oil plume edges resulted in contraction forces, which, however, did not substantially change the plume size due to the high molecular viscosity of the machine oil.

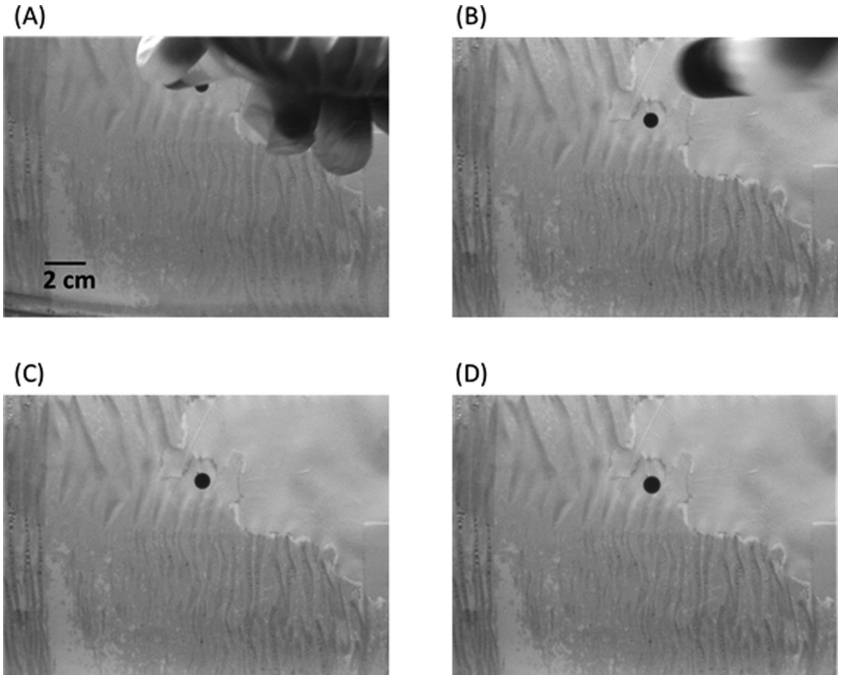

Figure 7. Machine oil slick (a) 0.33 s, (b) 0.60 s, (c) 1.00 s, and (d) 2.00 s after release on the water surface.

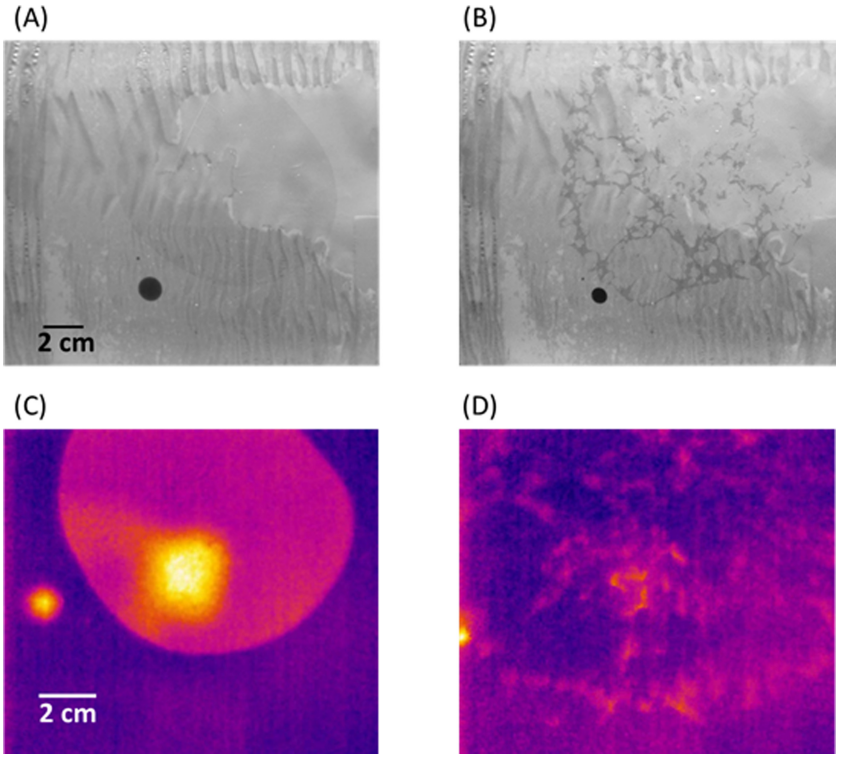

Figure 8. Crude and machine oil slicks 0.01 s before and 0.3 s after the application of the FFT-Solution^{TM} oil dispersant directly to the oil slick simultaneously in (a, b) visual and(c, d) infrared imagery. Note that the infrared imagery includes lamp and other object reflections.

3. Volume of Fluid Multiphase Model

For numerical simulation of the laboratory results described in section 2, we have developed a high-resolution, nonhydrostatic 3D multiphase modeling approach, which has been implemented with the computational fluid dynamics (CFD) software ANSYS *Fluent* 15.0.

The simulation was done in a numerical domain 0.04 m by 0.04 m in the horizontal, by 0.045 m in the vertical. The air layer had a thickness of 0.03 m, and the water layer, 0.015 m. The horizontal grid spacing was 2×10^{-4} m, while, the vertical spacing was 1×10^{-4} m at the air-water interface and gradually expanding to 1×10^{-3} m at the bottom of the water layer and to 1.8×10^{-3} m at the top of the air layer. The variable spacing was to save on the number of mesh elements.

The boundary conditions at the bottom and top of the numerical tank are specified as zero shear boundary conditions, which is equivalent to slippery boundary conditions. All four side walls were specified as no slip boundary conditions.

Figure 9 shows an example of an oil drop entering the water surface and the numerical mesh used for simulations. The spherical oil drop with radius 0.002 m was initially released from 0.026 m height above the water level. We selected the radius of 0.002 m in order to reproduce the results of the laboratory experiment. This radius is comparable to the crossover radius as defined by equation (3) and Table 3, which ensures that capillary forces are important.

Smaller drops would be more strongly affected by capillary forces. However, it could be difficult to simulate their expansion with the computational fluid dynamics model due to mesh resolution and computational limitations.

We used a large eddy simulation (LES) Wall-Adapting Local Eddy-Viscosity (WALE) turbulence model [*Nicoud and Ducros*, 1999] and a volume of fluid (VOF) multiphase model, which allowed us to simulate the air-water-oil interface including interfacial tensions and Marangoni forces. The multiphase model employed an explicit scheme for volume fraction with a volume fraction cutoff of 10^{-6}. The Marangoni effect was implemented via the interfacial tension force modeled with the *continuum surface stress* and *implicit body forces option* (see ANSYS Fluent 15.0 Theory Guide).

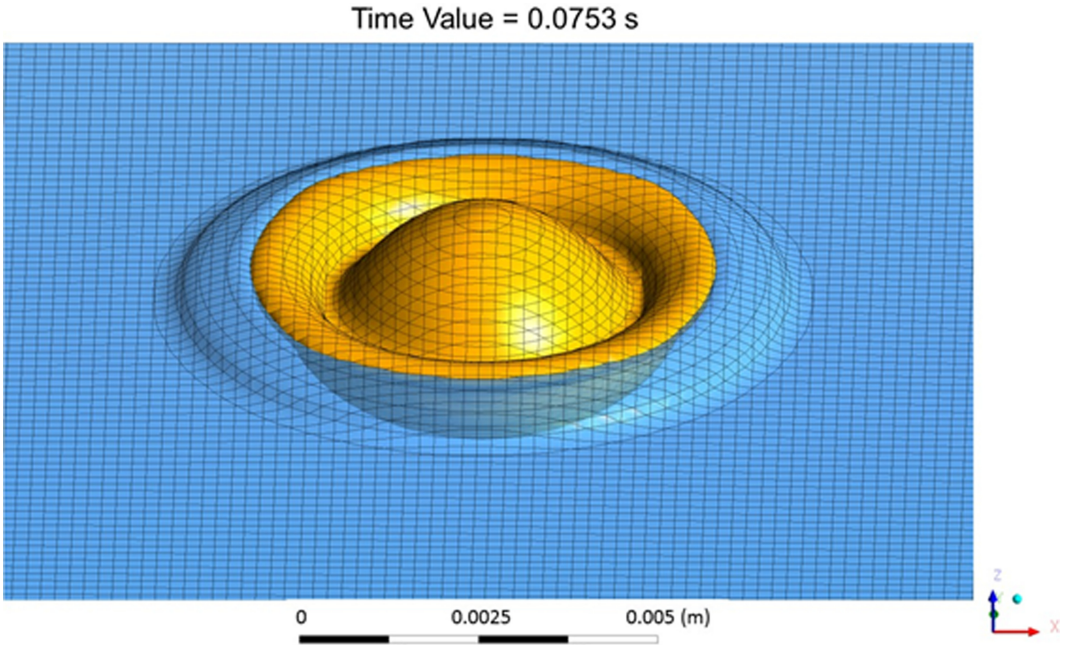

Figure 9. Oil drop splashing on the water surface. Yellow color corresponds to oil; blue, to water surface. Numerical mesh is also shown.

The VOF method models any number of immiscible fluids by solving an individual set of momentum equations and tracking the volume fraction of the separate fluids throughout the model domain. For these numerical simulations, three immiscible fluids were used (water, oil and air).

The VOF method tracks the volume fraction (α) of each of these fluids where any fraction of the q^{th} fluid is possible $(0 < \alpha_q < 1)$. The VOF method always ensures the sum is unity, $\alpha_{air}+\alpha_{water}+\alpha_{oil}=1$.

At the interfaces where more than one fluid in a cell is present, the VOF model uses the geometric interface reconstruction scheme, which is a piecewise-linear interpolation to calculate the advected fluid through each face [*Youngs*, 1982]. The tracking of the interface uses the following continuity equation:

$$\frac{1}{\rho_q}\left[\frac{\partial}{\partial t}\left(\alpha_q\rho_q\right)+\nabla\cdot\left(\alpha_q\rho_q\vec{v}_q\right)=S_{\alpha_q}+\sum_{p=1}^{n}\left(\dot{m}_{pq}-\dot{m}_{qp}\right)\right],$$

where ρ_q is the density of the q^{th} fluid, $\vec{v}_q$ is the velocity of the q^{th} fluid, $\dot{m}_{pq}$ is the mass transfer from the p^{th} to the q^{th} fluid and $\dot{m}_{qp}$ is the mass transfer from the q^{th} to the p^{th} fluid. S_{α_q} is a user-defined source term that remained at the default value of zero for our numerical simulations.

Table 3. Model Parameters[a]

Figure #	Water-Air Surface Tension Coefficient (Nm^{-1})	Oil-Air Surface Tension Coefficient (Nm^{-1})	Oil-Water Surface Tension Coefficient (Nm^{-1})	Dynamic Oil Viscosity μ ($kg\ m^{-1}s^{-1}$)	Crossover Radius r_c (m)	Comments
10, 14	0.072	0.028	0.019	0.01	0.003	Crude oil drop splashing
11a, 14				0.01		Crude oil slick spreading
11b, 14	0.001	0.028	0.019	0.01	0.003	Crude oil slick contraction due to dispersant
12, 14	0.072	0.032	0.04	0.40	0.0043	Machine oil drop piercing
13a, 14				0.40		Machine oil drop evolution
13b, 14	0.001	0.032	0.04	0.40	0.0043	Machine oil drop and dispersant
14	0.072	0.032	0.04	0.17	0.0043	Machine oil drop piercing
14				0.17		Machine oil drop evolution
14	0.001	0.032	0.04	0.17	0.0043	Machine oil drop and dispersant

[a]Air density is 1.225 kg m^{-3}, air viscosity is 1.789 10^{-5} kg $m^{-1}s^{-1}$, water density is 1021.5 kg m^{-3}, dynamic water viscosity is 0.00103 kg m^{-1} s^{-1}, and oil density is 876.5 kg m^{-3} for crude oil and 889 kg m^{-3} for machine oil. The crossover radius r_c determining transition from inertia to capillary regime is estimated according to equation (3).

The velocity field $\vec{u}$ calculated using the following equation:

$$\partial_t\left(\rho\vec{u}\right)+\nabla\cdot\left(\rho\vec{u}\,\vec{u}\right)=-\nabla p+\nabla\cdot\left[\mu\left(\nabla\vec{u}+\nabla\vec{u}^{\,T}\right)\right]+\rho\vec{g}+\vec{F}_{CSS}.$$

where ρ is the mixture density $(\rho=\alpha_{water}\rho_{water}+\alpha_{oil}\rho_{oil}+\alpha_{air}\rho_{air})$, μ is the dynamic viscosity $(\mu=\alpha_{water}\mu_{water}+\alpha_{oil}\mu_{oil}+\alpha_{air}\mu_{air})$, p is pressure, $\vec{g}$ is gravitational acceleration, and $\vec{F}_{CSS}$ is the surface tension force at each of the interfaces. The surface tension force is calculated using a continuum surface stress (CSS) derived from a stress tensor $T=\sigma(I-\hat{n}\otimes\hat{n})\,|\vec{n}\,|$, where σ is the surface tension, I is the unit tensor, $\otimes$ is the tensor product of the original normal and the transformed normal, $\vec{n}=\nabla\alpha$ and $\hat{n}=\vec{n}\,/|\vec{n}\,|$. The stress tensor ($T$) then becomes:

$T=\sigma(|\nabla\alpha|I-\frac{\nabla\alpha\otimes\nabla\alpha}{|\nabla\alpha|})$. The surface tension force is then determined as follows: $\vec{F}_{CSS}=\nabla\cdot T$.

In the CSS model, the curvature of the interface is not explicitly calculated but is instead represented as an anisotropic variant of modeling capillary forces based on surface stresses (ANSYS Fluent® version 15.0). For our simulations, the surface tension σ between air/water, air/oil, and water/oil were set as constants. In addition, air was chosen as the primary phase for computational stability.

More details on the multiphase VOF are found in *ANSYS, Inc*. [2013] and cited literature [*Hirt and Nichols*, 1981; *Youngs*, 1982].

4. Numerical Simulation of Air-Water-Oil Interfaces Coordinated With Laboratory Experiment

We have conducted numerical simulations to reproduce observations from the laboratory experiments with drops of crude and machine oil including application of dispersant. Table 3 contains pertinent information to these simulations.

Both oil and water phases may contain solutes that react to produce a surfactant at the drop interface [*Stocker and Bush*, 2007]. As a result, the oil-water surface tension may depend on chemical reactions of oil with water. Crude oil is expected to react much more intensely than machine oil due to a larger presence of volatile fractions. These reactions produce surfactants, which are adsorbed on the oil water interface, effectively reducing the interfacial tension between these two phases. However, if the surfactant is flushed away from the interface by a hydrodynamic process, the interfacial tension can increase.

The measurement of the crude (Macondo surrogate) oil-water interfacial tension has been done in *Murphy et al*. [2015]. The reported interfacial tension coefficient of the crude oil with seawater was changing over time decreasing from 0.018 to 0.008 N m^{-1}.

For modeling purposes, we set the crude oil-water interfacial tension at the oil-water interface equal to 0.019 Nm^{-1}. Due to the presence of the velocity shear at the interface during the continuous oil slick evolution in our lab experiment, the diffusion sublayer formed by surfactants released at the oil-water interface was effectively flushed away. For machine oil, we assume the oil-water interfacial tension is 0.04 Nm^{-1} and independent of the oil-water relative motion.

The crude (Macondo Surrogate) oil densities and viscosities are also taken from *Murphy et al*. [2015]. The remaining model material properties are given in the caption to Table 3.

4.1. Crude Oil

Figure 10a demonstrates the crude oil drop released 0.0026 m above the water surface. Figure 10b shows this drop entering the air-water interface and then producing a splash (Figure 10c). Further gravity spreading of the oil drop is shown in Figure 11a. The spreading factor for the crude oil calculated from equation (1) is equal to $S=0.025>0$. Due to the positive value of S, no equilibrium sessile lens can be formed. We have therefore implemented the assumption of *Amirfazli and Neumann* [2004] that at $S>0$ the triple junction line disappears and the effect of interfacial tension and tension of the triple junction line on the drop spreading vanishes. The interfacial tensions were discontinued for this stage, and the oil slick was spreading solely by buoyancy forces. The process of spreading was modeled until the crude oil drop spread into a surface oil film (Figure 11a) with thickness on the order of the vertical mesh resolution (0.0001 m).

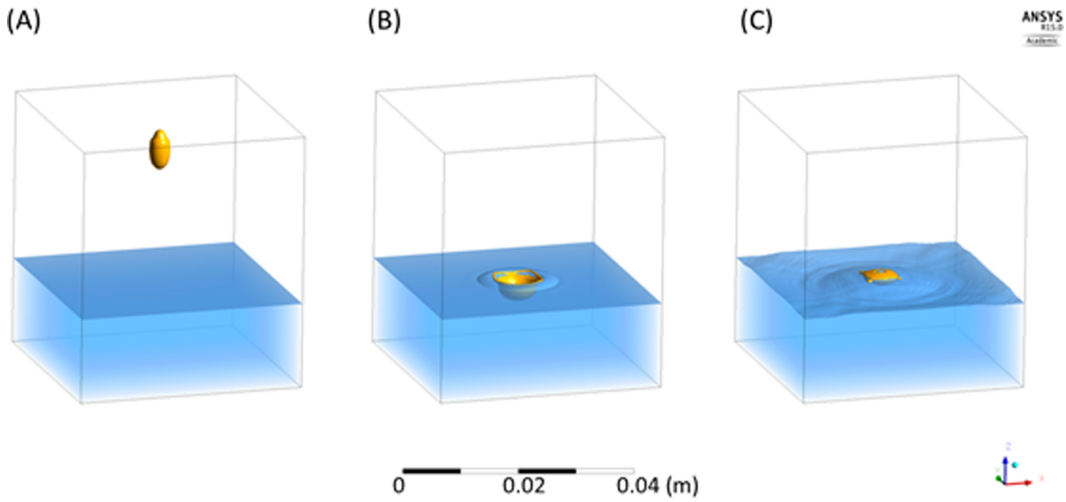

Figure 10. Simulation of dropping and splashing of the crude oil at (a) t=0.01 s, (b) t=0.078 s, and (c) t=0.144 s, where t is the elapsed time after the beginning of the simulation.

An alternative interpretation of lens spreading at positive values of S in the form of precursor film [*Dipietro et al.*, 1978; *Foda and Cox*, 1980] was not feasible to implement in the numeric model due to mesh size limitations, requiring micrometer size resolution.

Application of dispersant to the outside of the oil slick was simulated in the model by reduction of the air-water surface tension from 0.072 Nm^{-1} to 0.001 Nm^{-1}. This resulted in a rapid contraction of the crude oil slick by the interfacial tension force (Figure 11b), which can be interpreted as the Marangoni force because it is caused by the gradient of surface tension along the near air-water-oil horizontal surface. This simulation corresponds to the laboratory observations reported in Figure 5. The contraction of the crude oil slick is an "explosive" type process, which takes place within a few tenths of a second. This is consistent with the laboratory observation.

4.2. Machine Oil

In the numerical simulation, the machine oil drop pierced the air-water interface with relatively little spreading (Figures 12a–12c). The drop entered the water almost like a rigid body. No significant spreading (Figure 13a) or contraction (Figure 13b) due to the effect of dispersant were observed.

Remarkably, the machine oil drop gradually migrated to the numerical tank wall due to the Marangoni effect and "glued" to it (Figure 13b). This is consistent with the laboratory observations shown in Figure 5c.

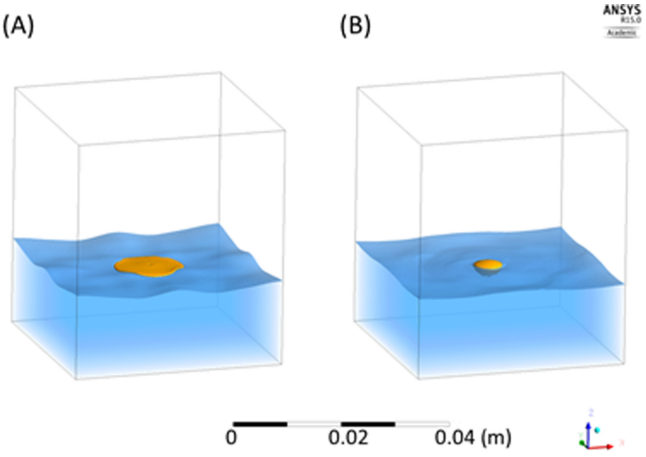

Figure 11. Simulation of the effect of dispersants on crude oil slick: (a) before (t=0.6 s) and (b) after (t=0.8 s) the application of the dispersant.

The full solution including both physical and chemical aspects of this problem was not feasible at this point. Consequently, we had to introduce some simplifications in our model. In particular, we did not directly include in the model chemical reactions producing surfactants at the oil drop surface, but included them parametrically. Notably, the surfactants can significantly affect spreading of the oil on the sea surface; which, however, was expected from laboratory experiments to be more important for crude oil than for machine oil. We also did not include the leading precursor film in the

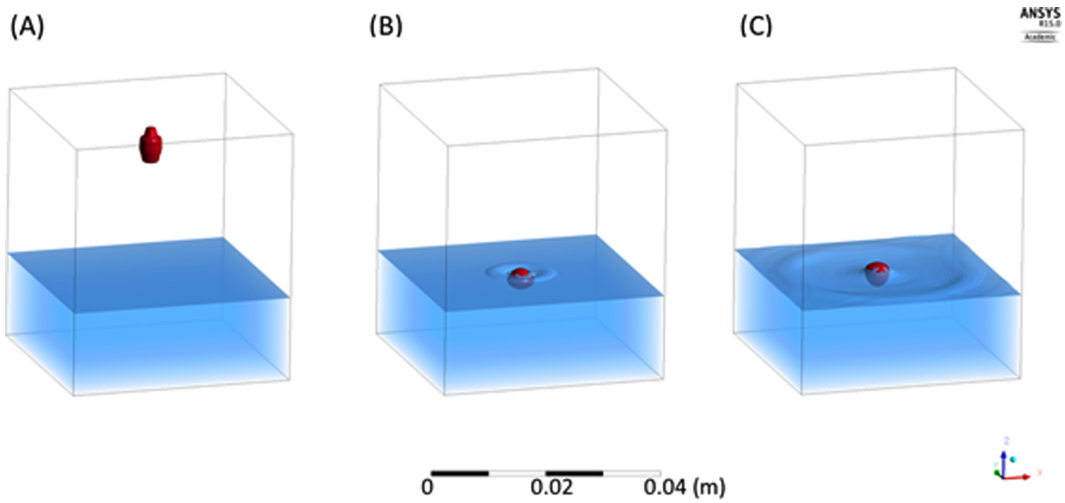

Figure 12. Simulation of dropping and splashing of the machine oil drop at (a) t=0.0109 s, (b) t=0.1009 s, and (c) t=0.1449 s.

numerical simulation. This film is a monomolecular layer and its simulation requires a nanometer mesh resolution, which is not feasible at this point.

5. Discussion

The initial laboratory experiment, conducted on 13 May 2014 (Figures 4 and 5), though largely qualitative, helped us understand the difference between dynamics of crude and machine oil, including application of dispersant. The experiment on 15 October 2015 was conducted in seawater and included specialized cameras to allow quantification of the slick dimension evolution. In parallel with the laboratory experiment on 15 October 2015, we also performed a 3D multiphase numerical simulation of small-scale surface dynamics of oil slicks, including the application of dispersant.

The numerical simulation continued during 0.6 s, until the thickness of the spreading plume reached the limit of the vertical mesh resolution. Then, dispersant was introduced in the simulation. At the same time, the laboratory experiments included spreading of the oil drop for several seconds before dispersant was applied. The comparison between lab and numerical experiments was therefore done during the first 0.6 s.

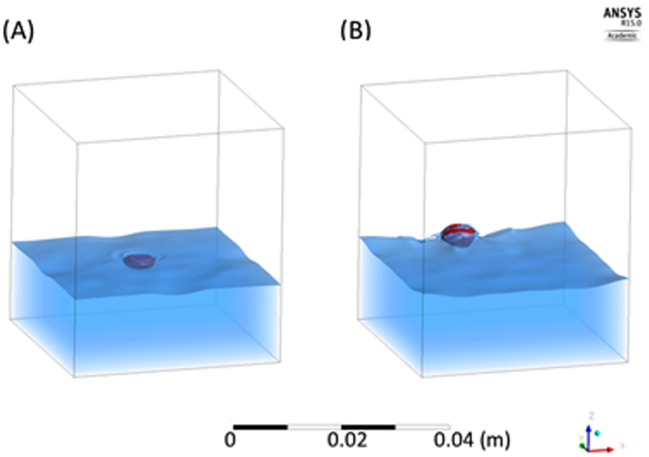

Figure 13. Simulation of the effect of dispersants on machine oil drop: (a) before (t=0.6 s) and (b) after (t=0.8 s) the application of the dispersant.

The numerical results for crude and machine oil appear to be qualitatively and to some extent quantitatively consistent with the results of the laboratory experiments. Notably, the evolution of the diameter of the crude and machine oil drops in the process of spreading and rapid contraction of the oil slick after dispersant application to the water surface is consistent between laboratory and numerical experiments (Figure 14).

In the laboratory experiments and numerical simulations, the first stage of a crude oil slick spreading was due to the oil drop splash on the water surface after its release at a several centimeter height above the water surface

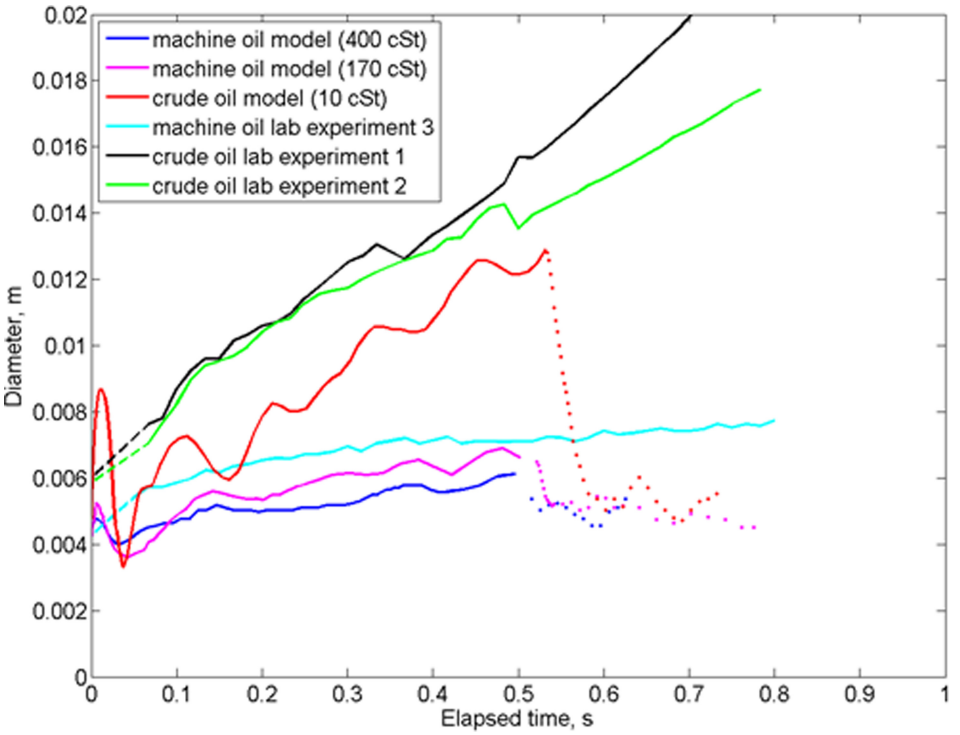

Figure 14. Diameter of crude and machine oil drops in the process of spreading and contraction on the water surface as a result of numerical simulations and laboratory experiments. Elapsed time is referenced according to the first contact of the falling drop with the water surface. The laboratory experiment numbers correspond to the case numbers in Table 2. The dotted lines correspond to the model slick contraction due to application of dispersant, 0.6 s after beginning of the simulation. Application of dispersant in the laboratory experiment, shown in Figures 5 and 8, took place later than 1 s and, therefore, is not a part of the graph.

(Figures 4, 6 and 10). As a result of the initial release from the air, a sessile oil lens formed on the water surface. The initial radius of the sessile lens was 2.9 mm, which was close to the numerical simulation results. The next stage included spreading of the sessile oil lens 11 a).

In contrast, the drop of machine oil pierced the water surface almost like a rigid body, practically with no splash, which was due to relatively large viscosity of machine oil. The radius of the machine oil drop was 2.1 mm after entering the water. Only relatively small subsequent spreading was observed in this case both in the laboratory experiment (Figures 4 and 7) and numerical simulation (Figure 12).

In the numerical simulation, the minimum diameter point observed around 0.03 s (Figure 14) was due to the oil drop oscillation after impact with the water surface and surface waves reflected from the boundaries of the numerical domain. Note that the laboratory tank had larger horizontal dimension and the effect of reflected waves was not so pronounced. The drop size oscillations were more pronounced for the crude oil because of the lower molecular viscosity. In the laboratory data, the image of the oil drop during the first $\sim$0.06 s was obscured by the hand of the investigator. In Figure 14, the interval from 0 to 0.06 s was therefore interpolated and shown as dashed lines.

The crossover radius of oil drops for which surface tension effects become important, as estimated in Table 3 by equation (3), was 3 mm for crude oil and 4.3 mm for machine oil for the reported laboratory and related numerical experiments. The size of the oil droplets in the laboratory and numerical experiments was selected based on these estimates.

Application of dispersant to the crude oil resulted in an "explosive" type processes leading to in a rapid contraction or fragmentation of the oil film into narrow wedges and small droplets (Figures 5, 8 and 11). In contrast, application of dispersant to the machine oil patch did not produce any dramatic effect either in the laboratory experiment or in the computational fluid dynamics simulation (Figures 5, 8 and 13). As mentioned above, machine oil has a much larger molecular viscosity than crude oil and, respectively, a much larger response time to interfacial tension forces.

Dispersant, when applied to the water surface outside the crude oil slick resulted in a rapid slick contraction. At the same time, dispersant sprayed directly on the crude oil slick fragmented the slick into multiple narrow wedges and tiny drops.

Interfacial tension forces appear to be a critical component in the process of oil dispersion into micrometer scale droplets. When mixing due to shear, wave breaking, or gravitational convection occurs in the upper layer of the ocean, the dispersant-treated oil slick breaks up into many tiny droplets that are less than 100 μm in diameter. Fragmentation of oil spills due to turbulent mixing, however, is limited by the Kolmogov's internal scale of turbulence, which is of the order of a few millimeters in the ocean. There is no effective turbulent mixing below this length scale. On sub-millimeter scales, the process of dispersion is dominated by surface tension forces, which include both normal and tangential (Marangoni) components.

Due to the action of mechanical force, dispersant-treated oil slicks break up into many tiny droplets. Dispersants contain surfactants and solvents. Surfactant molecules have one hydrophobic end and one hydrophilic end. Being aligned at the air-water or oil-water interface, surfactants reduce interfacial tensions. According to the traditional interpretation, dispersants enhance mechanical breakup of the oil slick due to surface tension reduction. The oil droplet radius depends on interfacial tension, increasing with the reduction of the latter. The oil-water interfacial tension is, however, much reduced by the effect of dispersants, which would prevent development of the small oil droplets observed in reality after the application of dispersant. This contradiction remaining in the traditional conceptual theory can be resolved by taking into account the Marangoni force. According to *Tseng and Prosperetti* [2015], the mechanical breakup of the oil spill due to wave breaking and shear in the near-surface layer initially fragments the oil spill into irregular fragments, which contain near zero vorticity points. Interfacial tension in near zero vorticity points is reduced due to formation of micrometer-thick surfactant diffusion sublayers at the oil-water interface. The surfactant diffusion sublayer is effectively flushed away in nonzero vorticity points, increasing the interfacial tension. Subsequent development of large interfacial tension gradients near zero vorticity points initiates the Marangoni force, which finally fragments the oil spill into tiny oil droplets. This process resembles the *Bush* [2013] mechanism schematically illustrated in Figure 2.

Transport of an oil spill on the sea surface can depend on the oil age and application of dispersants. Thin surface oil slicks produced by crude oil are transported by the surface drift motion due to wind action and Stokes drift. Drops and lenses, typical for weathered oil, may extend vertically across the aqueous viscous sublayer and drift with somewhat different velocity. This difference depends on wind-wave conditions and may achieve several centimeters per second [*Soloviev and Lukas*, 2014]. At the same time, the oil dispersed in the water column will propagate within the upper ocean turbulent boundary and is subject to the effect of wave breaking, Langmuir circulation, shear, and convection.

Incorporation of the interfacial tension forces including Marangoni effects into existing theories can help to elucidate the oil spill transport and dispersion processes. This statement is supported by the laboratory experiment and numerical simulations presented in this paper.

After oil spill incidents, like Deepwater Horizon, large areas of the sea surface are covered with oil slicks, some of them, of millimeter or sub-millimeter scale thickness [*National Research Council*, 2003]. In the ocean environment, oil spills are subjected to wind/wave mixing, near surface currents, chemical reactions of oil with saltwater and dispersants, evaporation, dissolution, and emulsification. Small-scale physics including capillarity effects are inherently involved in these processes but have not yet been consistently incorporated into the existing oil spill models. Combined laboratory and numerical experiments can help to develop more realistic subgrid-scale parameterizations and account for the missing physics in operational oil-spill transport and dispersion models.

6. Conclusions

In this work, we conducted laboratory experiments demonstrating the difference between crude and weathered oil spill dynamics on small scales, including the effect of dispersants. After deposition on the still water surface, a drop of crude oil quickly spread into a thin film; while, a drop of weathered (machine) oil did not show such significant evolution. Application of dispersant to the water surface around the crude oil slick resulted in a quick slick recoiling. In contrast, dispersant sprayed directly on the crude oil slick

fragmented the slick into multiple narrow wedges and tiny drops. The drop of machine oil nevertheless did not show significant change in size or topology after spraying dispersant either on the surrounding water surface or directly on the oil plume. This difference may have some consequences for aerial dispersant application during oil spill response.

In addition, we reproduced some lab experiment results using a computational fluid dynamics model. A multi-phase, volume of fluid computational fluid dynamics model incorporating capillary forces was able to explain some features observed in the laboratory experiment, including the spreading of crude oil slicks and their contraction after dispersant was applied outside of the slick.

The laboratory and numerical experiments are inherently limited in temporal and spatial scales and practical application of the results may be a challenge. Nevertheless, as we have seen from equation (3) and Table 3, the interfacial capillary length is on the order of millimeters. This indicates that on microscale, the capillary effects can be comparable to, or dominant over wind-wave forcing. The laboratory and numerical results, which are obtained within the limited temporal and spatial scales, can be applicable to oil spill dynamics in the open ocean conditions without scaling.

We have demonstrated critical importance of capillary forces for oil spill transport and dispersion, and a new interpretation of the effect of dispersant on the oil dispersion process incorporating the Marangoni effect has been developed.

Acknowledgments

The authors are grateful to Joseph Katz (JHU) for guidance on Macondo surrogate oil properties. James H. "Rip" Kirby III (USF) kindly provided samples of the FFT-Solution™ oil dispersant and detailed directions on its application. We thank Michael Rebozo (UM) for excellent technical support of the lab experiment, Kathryn Howe (NSU) for help in the laboratory and numerical data processing, and Jeremy McCaslin (ANSYS) for discussion of multiphase physics incorporated in FLUENT. This research was made possible by a grant from the Gulf of Mexico Research Initiative to Consortium for Advanced Research on Transport of Hydrocarbon in the Environment (CARTHE). The laboratory and numerical data can be found in GRIIDC at https://data.gulfresearchinitiative.org/data/R4.x265.239:0002 and https://data.gulfresearchinitiative.org/data/R4.x265.240:0003, respectively.

References

Amirfazli, A., and A. W. Neumann (2004), Status of the three-phase line tension, *Adv. Colloid Interface Sci.*, *110*, 121–141.

ANSYS, Inc. (2013), *ANSYS FLUENT 15.0 Theory Guide*, Canonsburg, Pa.

Bacri, L., G. Debregeas, and F. Brochard-Wyart (1996), Experimental study of the spreading of a viscous droplet on a nonviscous liquid, *Langmuir*, *12*, 6708–6711.

Bush, J. W. M. (2013), Interfacial phenomena, MIT OCW, 18.357, 80.

Dipietro, N. D., C. Huh, and R. G. Cox (1978), The hydrodynamics of the spreading of one liquid on the surface of another, *J. Fluid Mech.*, *84*(3), 529–549.

Eggers, J. (1997), Nonlinear dynamics and breakup of free-surface flows, *Rev. Mod. Phys.*, *69*(3), 865–930.

Fannelop, T. K., and G. D. Waldman (1972), Dynamics of oil slicks, *Am. Inst. Aeronaut. Astronaut. J.*, *10*(3), 506–510.

Fay, J. A. (1969), The spread of oil slicks on a calm sea, in *Oil in the Sea*, edited by D. Hoult, pp. 53–63, Plenum, N. Y.

Foda, M., and R. G. Cox (1980), Spreading of thin liquid films on a water-air interface, *J. Fluid Mech.*, *101*(1), 33–51.

Franklin, B. (1774), Of the stilling of waves by means of oil, *Philos. Trans. R. Soc. London B*, *64*, 445–460.

Gibbs, J. W. (1961), *The Scientific Papers of JW Gibbs*, vol. 1., 288 pp., Dover, N. Y.

Harkins, W. D. (1952), *The Physical Chemistry of Surface Films*, Reinhold, N. Y.

Hirt, C. W., and B. D. Nichols (1981), Volume of fluid (VOF) method for the dynamics of free boundary, *J. Comput. Phys.*, *39*, 201–225.

Hoult, D. P. (1972), Oil spreading on the sea, *Annu. Rev. Fluid Mech.*, *4*, 341–367.

Joye, S., and I. MacDonald (2010), Offshore oceanic impacts from the BP oil spill, *Nat. Geosci.*, *3*(7), 446.

Langmuir, I. (1933), Oil lenses on water and the nature of monomolecular expanded films, *J. Chem. Phys.*, *1*, 756–776.

Miksis, M. J., and J. M. Vanden-Broeck (2001), Motion of a triple junction, *J. Fluid Mech.*, *437*, 385–394.

Murphy, D., C. Li, V. d'Albignac, D. Morra, and J. Katz (2015), Splash behaviour and oily marine aerosol production by raindrops impacting oil slicks, *J. Fluid Mech.*, *780*, 536–577.

National Research Council (2003), *Oil in the Sea III: Inputs, Fates, and Effects*, Natl. Acad. Press, N. Y.

Nicoud, F., and F. Ducros (1999), Subgrid-scale stress modelling based on the square of the velocity gradient tensor, *Flow Turbul. Combust.*, *62*, 183–200, doi:10.1023/A:1009995426001.

Pismen, L. M. (2002), Interfacial phenomena and the marangoni effect, in *Static and Dynamic Three-Phase Contact Lines*, vol. 428, edited by M. G. Velarde and R. K. Zeytourian, pp. 1–39 Springer, Vienna, Austria.

Pujado, P. R., and L. E. Scriven (1972), Sessile lenticular configuratiosn: Translationally and rotational symmetric lenses, *J. Colloid Interface Sci.*, *40*(1), 82–98.

Rowlinson, J. S., and B. Widom (1982), *Molecular Theory of Capillarity*, Clarendon, Oxford, U. K.

Soloviev, A., and R. Lukas (2014), *The Near-Surface Layer of the Ocean: Structure, Dynamics and Applications*, Springer, Berlin.

Stachowiak, G., A. W. Batchelor, and A. W. Batchelor (2011), *Engineering Tribology*, 801 pp., Butterworth-Heinemann, Burlington, Vermont.

Stocker, R., and J. Bush (2007), Spontaneous oscillations of a sessile lens, *J. Fluid Mech.*, *583*, 465–475.

Tam, D., V. Von Armin, G. H. McKinley, and A. E. Hosoi (2009), Marangoni convection in droplets on superhydrophobic surfaces. *J. Fluid Mech.*, *624*, 101–123.

Tseng, Y. H., and A. Prosperetti (2015), Local interfacial stability near a zero vorticity point, *J. Fluid Mech.*,*776*, 5–36.

van Nierop, E. A., A. Ajdari, and H. A. Ston (2006), Reactive spreading and recoil pf oil on water, *Phys. Fluids*, *18*, 038105.

Youngs, D. L. (1982), Time-dependent multi-material flow with large fluid distortion, in *Numerical Methods for Fluid Dynamics*, edited by K. W. Morton and M. J. Baines, pp. 273–285, Academic, N. Y.